ASTRONOMY & ASTROPHYSICS
SUPPLEMENT SERIES

Astron. Astrophys. Suppl. Ser. **127,** 185-200 (1998)

SiO masers in OH/IR stars, proto–planetary and planetary nebulae⋆

L.–Å. Nyman[1,2], P.J. Hall[3], and H. Olofsson[4]

[1] ESO/La Silla, Casilla 19001, Santiago 19, Chile
[2] Onsala Space Observatory, S–439 92 Onsala, Sweden
[3] Australia Telescope National Facility, PO Box 76, Epping, NSW 2121, Australia
[4] Stockholm Observatory, S–133 36 Saltsjöbaden, Sweden

Received February 28, 1996; accepted May 5, 1997

Abstract. We present a search for SiO masers towards a sample of 126 objects including OH/IR stars, proto–planetary and planetary nebulae. All objects are classified as oxygen–rich, and most of them are associated with OH or H_2O masers. SiO masers were found only in variable objects like the OH/IR stars and a few objects classified as proto–planetary nebulae, but with variable central stars that may be part of binary systems. In one object, OH 15.7+0.8, which appears to be varying irregularly and most likely recently left the AGB, an SiO maser was tentatively detected. Thus, we conclude that variability and SiO maser emission are closely linked, and that SiO masers disappear very soon after a star has reached the end of the AGB, when pulsation and mass loss cease.

Key words: stars: AGB and post-AGB — masers — radio lines: stars

1. Introduction

SiO, H_2O, and OH masers have been found to be associated with stars on the Asymptotic Giant Branch (AGB), as well as with post–AGB stars. The masers are located in the circumstellar envelopes, with the SiO masers closest to the star (and possibly even inside the expanding envelope) and the OH masers furthest away. All three types of masers are usually found around stars presently losing mass, e.g. Mira variables and OH/IR stars. However, when the mass loss stops the H_2O and SiO masers disappear, whereas the OH masers remain active also during the proto–planetary (PPN) and early planetary nebula (PN) stages (Lewis 1989).

OH and H_2O masers have been studied in several surveys towards late–AGB and post–AGB objects (e.g., Likkel 1989; Hu et al. 1994), but relatively little work has been done on the late evolution of SiO masers. Gomez et al. (1990) observed SiO ($v = 1$, $J = 1 - 0$) and H_2O masers in OH/IR stars and a few PPNe and found that the detection rate of both masers drops with increasing IRAS [25–12] color, which is believed to be an evolutionary stage indicator. Observations of SiO masers in OH/IR stars were also done by Jewell et al. (1991), and Nyman et al. (1986; 1993a). SiO masers have only been found towards four objects classified as PPNe, and they are discussed in Sect. 5.

To investigate more thoroughly the evolution of SiO masers we have searched for SiO emission towards a large sample of OH/IR stars with cool envelopes, oxygen–rich PPNe, and young PNe. The search was done in three different transitions, SiO ($v = 1$ and 2, $J = 1-0$) at 43 GHz, and SiO ($v = 1$, $J = 2 - 1$) at 86 GHz, because, although all transitions produce bright masers in Mira variables, there are indications that the SiO ($v = 1$, $J = 1 - 0$ and $J = 2-1$) masers are underluminous in OH/IR stars with cool envelopes (Nyman et al. 1993a).

2. The sample

The sample consists of 126 objects. It includes OH/IR stars with cool envelopes, PPNe that are believed to be oxygen–rich (i.e. they are associated with OH or H_2O masers, and/or the central stars are of spectral class M, and/or they have silicon dust features in the infrared spectra), and PNe associated with OH–masers. Five of the objects are more likely to be pre–main sequence objects than evolved objects, but were observed nevertheless. They are included in Table 1 (labeled "PMS?") and Table 2, but

Send offprint requests to: L.–Å. Nyman (ESO address)

⋆ Tables 1 and 2 are available at the CDS via anonymous ftp 130.79.128.5 or via http://cdsweb.u-strasbg.fr/Abstract.html and Fig. 1 can be found in the on-line version of A&AS via http://www.ed-phys.fr

are not taken into account in the rest of the paper. The sample that is being discussed thus consists of 121 objects.

The objects with cool envelopes were mainly selected from Likkel (1989), Likkel et al. (1991), Omont et al. (1993), and Silva et al. (1993), and OH/IR stars as well as PPNe are included.

More post–AGB candidates were selected from the literature and they can be divided into the following categories:

1. Non–variable OH/IR stars (Herman & Habing 1985; van Langevelde et al. 1990).
2. High–velocity OH or H_2O maser sources (te Lintel Hekkert et al. 1988, 1992; te Lintel Hekkert 1991; Likkel et al. 1992). In these objects the velocity extent of the maser emission imply motions with velocities larger than the largest envelope expansion velocities expected for stars on the AGB (about 40 km s^{-1}).
3. Objects where the velocity width of the H_2O maser emission exceeds that of the OH emission, indicating that the objects recently have become PPNe (Gomez et al. 1994).
4. Early type stars and/or objects with a double–peaked energy distribution. In some cases there is an association with an OH maser (Hu et al. 1993a, 1994).
5. Low–excitation emission line objects (Hen 1191 and Hen 1379, Le Bertre et al. 1989; M1–92 and M2–56, Bujarrabal et al. 1992).
6. Some sources that are considered to be oxygen–rich post–AGB objects: the Frosty Leo nebula (Forveille et al. 1987), HR 3126 (Chiar et al. 1993; Nyman et al. 1993b), Roberts 22 (Silva et al. 1993), and IRAS 07131 − 0147 (Scarrott et al. 1990).

The PNe were selected from Zijlstra et al. (1989, 1991). For two PNe there were significant differences between the radio continuum and OH maser positions, and therefore both positions were observed.

Table 1 lists the sources, observed positions, center velocities of the spectra, presence of maser emission (the detections made in this work are included, and our new detections are marked with a capital "X"), the evolutionary status of the object, and references to papers from which the sources were selected and to SiO maser data. The evolutionary status of the objects given in Table 1 have been classified in the following ways:

1. OH/IR: objects with double–peaked OH spectra that have been found to have variable OH, and/or optical, and/or infrared emission. If no special monitor observations have been reported in the literature, we regard an object as variable if the IRAS variability index is > 90. None of the characteristics given below for PPNe have been reported for these objects.
2. PPN: objects that have one or more of the following characteristics: bipolar appearance, an early type central star, a double peaked energy distribution, high velocity masers, and/or the velocity width of the H_2O emission exceeds that of the OH emission.
3. PN: Objects that have been detected in radio continuum, indicating the presence of ionized gas.
4. Two objects where OH maser emission has not been detected, but with variable central stars are labeled as "variable star".
5. Two objects are labeled "supergiant": IRAS 22480+6002 that has been classified as a supergiant (Winfrey et al. 1994), and IRC+10420 which may be a post–AGB object or a supergiant (e.g. Oudmaijer et al. 1994).

These definitions cover 86% of the sample. The rest of the objects do not fit into the above criteria because of lack of relevant observations. We have not made any attempt to separate them into possible OH/IR objects or PPNe, although most of them probably are OH/IR objects. They are labeled "?" in Table 1.

The OH/IR stars most likely contain a mixture of AGB stars, supergiants, and perhaps also a few very young PPNe that have just started to evolve off the AGB. The objects classified as PPNe most likely consist of PPNe at different ages as well as a objects that may not be true PPNe, e.g. some of the binary systems that produce bipolar nebulae.

The sample roughly consists of 37% variable stars (mostly OH/IR objects), 36% PPNe, 13% PNe, and 14% unclassified objects.

3. Observations

3.1. SiO 43 GHz observations

Observations at the 43 GHz SiO ($v = 1$ and 2, $J = 1 - 0$) transitions were made using the Parkes radio telescope during the period September 16–21, 1993. At 43 GHz the inner 16.7 m of the 64 m reflector is effectively used and, with an aperture efficiency of 34%, the telescope sensitivity is 39 Jy K^{-1}. The beam size at 43 GHz is $1'.6$. Telescope pointing errors are less than $12''$ (rms) in right ascension and declination.

We used the CSIRO 43 GHz maser superheterodyne receiver, giving typical system temperatures in the range $90 - 120$ K (SSB). All observations were made in horizontal linear polarization. The instantaneous bandwidth of the maser RF amplifier was about 100 MHz, precluding simultaneous observations of the $v = 1$ and $v = 2$ transitions.

Measured fluxes were corrected for atmospheric attenuation using the form $\exp(\tau \cdot s(Z))$, where Z is the telescope zenith angle and τ, the vertical attenuation, was taken as 0.1. During the first few days of the observations the weather was unstable with clouds and occasional rain showers making the calibration uncertain. Apart from the data taken during unstable weather conditions, we estimate that the flux values are accurate to ±20%.

Table 1. Source parameters

IRAS name	Other name	Ra (1950)	Dec (1950)	$V_{\rm lsr}$	OH	H_2O	SiO	Type	Reference
01304 + 6211	OH 127.8 − 0.02	01h30m27.0s	+62°11′25″	−55	x	x	x	OH/IR	1, 5
03206 + 6521	OH 138.0+7.2	03h20m41.6s	+65°21′31″	−37	x		x	OH/IR	2, 5
03293 + 6010	OH 141.7+3.5	03h29m23.6s	+60°10′04″	−57	x	x	x	OH/IR	2, 6, 9
04361 + 2547		04h36m09.4s	+25°47′27″	6	x	x		PMS?	1
06319 − 0501	AFGL 5201	06h31m58.3s	−05°01′13″	−60	x	x		OH/IR	1
06530 − 0213		06h53m00.9s	−02°13′35″	28	x			PPN	1, 10, 11
07027 − 7934		07h02m45.3s	−79°34′22″	−27	x			PN	12
07131 − 0147		07h13m10.9s	−01°47′23″	0				PPN	13
07180 − 1314	AFGL 5229	07h18m00.7s	−13°14′33″	0	x	x	X	OH/IR	2, 9
07399 − 1435	OH 231.8+4.2	07h39m58.9s	−14°35′43″	40	x	x	x	PPN	5, 9, 32
07536 − 2830	HU Pup	07h53m38.6s	−28°30′55″	0	x	x	X	OH/IR	2, 9
07559 − 5859	HR 3126	07h55m54.5s	−58°59′21″	0				PPN	28
08005 − 2356		08h00m32.5s	−23°56′16″	0	x			PPN	1, 10, 22
08357 − 1013	OH 235.3+18.1	08h35m44.5s	−10°13′43″	0	x	x	X	?	2, 9
09371 + 1212	Frosty Leo	09h37m11.2s	+12°12′30″	−20				PPN	1, 30, 31
09429 − 2148	IRC-20197	09h42m58.3s	−21°48′05″	40	x	x	x	OH/IR	2, 9, 23
10197 − 5750	Roberts 22	10h19m45.1s	−57°50′28″	0	x			PPN	3
11385 − 5517	HD 101584	11h38m33.6s	−55°17′46″	40	x			PPN	29
11516 − 6201		11h51m36.6s	−62°02′00″	20	x			?	3
12358 − 6323		12h35m53.0s	−63°23′09″	−3	x			?	10, 11
14086 − 0730		14h08m38.9s	−07°30′45″	−26	x		X	OH/IR	2, 9
14122 − 5947		14h12m14.0s	−59°47′25″	0				PN	10, 37
14341 − 6211		14h34m10.7s	−62°11′42″	−23	x			PPN	10, 11
15405 − 4945		15h40m32.1s	−49°45′54″	50	x			PPN	14
16029 − 3041	OH 345.0+15.7	16h02m59.7s	−30°41′30″	−4	x		x	?	2, 9, 41
16086 − 5255		16h08m37.8s	−52°55′37″	0				PPN	10
16235 − 4832	Hen1191	16h23m31.8s	−48°32′45″	−9				PPN	15
16342 − 3814		16h34m17.1s	−38°14′18″	50	x			PPN	14
16559 − 2957		16h55m57.3s	−29°57′11″	56	x			PPN	1, 10, 11
16594 − 4656		16h59m26.7s	−46°56′14″	−26				PPN	16
17103 − 3702	NGC 6302	17h10m21.3s	−37°02′43″	−40	x			PN	4
17106 − 3046		17h10m39.0s	−30°46′13″	6	x			?	3
17118 − 2952		17h11m53.0s	−29°52′53″	−40	x			OH/IR	1
17150 − 3754	OH 349.36−0.20	17h15m04.0s	−37°54′54″	−125	x			PN	4
17150 − 3224		17h15m04.6s	−32°24′15″	26	x			PPN	10, 11, 26
17163 − 3907	Hen1379	17h16m22.0s	−39°07′36″	5				PPN	15
17195 − 2710		17h19m35.5s	−27°10′45″	0				PPN	10
17207 − 2856		17h20m44.7s	−28°55′52″	−20	x			PN	4
17221 − 3038	PK 356+2.1	17h22m06.1s	−30°38′05″	0	x			PN	4
17233 − 2602	OH 0.1+5.1	17h23m23.0s	−26°02′27″	−143	x			PPN	10, 11
17292 − 2727		17h29m15.4s	−27°27′54″	−50	x			?	1
17317 − 2743	OH 359.8+2.6	17h31m44.9s	−27°43′16″	45	x			?	1
17347 − 3139		17h34m45.9s	−31°39′11″	−100	x			PN	4
17360 − 3012	OH 358.16+0.5	17h36m02.3s	−30°12′49″	2	x		x	OH/IR	2, 7
17371 − 2747		17h37m11.8s	−27°48′38″	115				PN (continuum pos.)	4
17371 − 2747		17h37m08.4s	−27°48′30″	115	x			PN (OH maser pos.)	4
17375 − 2759		17h37m29.4s	−27°59′29″	30				PN (continuum pos.)	4
17375 − 2759		17h37m26.7s	−28°00′04″	30	x			PN (OH maser pos.)	4
17375 − 3000		17h37m32.6s	−30°00′29″	0	x			PN	4
17385 − 3332		17h38m34.4s	−33°32′14″	−236	x			PPN	10, 11
17393 − 2727	OH 0.9+1.3	17h39m24.7s	−27°27′02″	−110	x			PN	4
17404 − 2713	OH 1.2+1.3	17h40m29.5s	−27°13′26″	0	x			PPN	10, 11
17411 − 3154		17h41m07.4s	−31°54′24″	−20	x		X	OH/IR	2, 3, 9
17423 − 1755	He 3−1475	17h42m18.8s	−17°55′36″	45	x			PPN	17, 38

Table 1. continued

IRAS name	Other name	Ra (1950)	Dec (1950)	$V_{\rm lsr}$	OH	H_2O	SiO	Type	Reference
17433 − 1750		17h43m20.6s	−17°50′43″	120	x			PPN	1, 10, 11
17443 − 2519		17h44m22.2s	−25°19′15″	29	x			OH/IR	2
17443 − 2949		17h44m23.8s	−29°49′44″	−10	x			PN	4
17459 − 3057		17h45m56.5s	−30°57′27″	6	x		X	OH/IR	2, 9
17484 − 1511		17h48m28.2s	−15°11′41″	94	x			?	1
17505 − 3143		17h50m31.5s	−31°43′52″	4	x		X	OH/IR	2, 9
17516 − 2525		17h51m37.8s	−25°26′00″	−15	x			PPN	2, 24
17534 + 2603	89 Her	17h53m24.0s	+26°03′23″	−5				PPN	27, 33
17565 − 2035		17h56m35.7s	−20°35′56″	204	x			?	2
17579 − 3121		17h57m59.1s	−31°21′55″	10	x			PPN	3
17580 − 3111		17h58m08.0s	−31°10′27″	20	x			PN	4
18016 − 2743		18h01m35.0s	−27°43′26″	74	x			PPN	10, 11
18025 − 3906		18h02m35.0s	−39°06′16″	−116	x			PPN	3
18044 − 1947		18h04m29.1s	−19°47′06″	0	x			OH/IR	2
18055 − 1833	AX Sgr	18h05m31.4s	−18°33′38″	0	x			OH/IR	2, 40
18071 − 1727	OH 12.8+0.9	18h07m11.1s	−17°27′13″	24	x			PPN	2, 24
18081 − 0338		18h08m11.1s	−03°38′56″	7	x			OH/IR	18
18095 + 2704		18h09m30.9s	+27°04′28″	0	x			PPN	2, 25
18105 − 1935		18h10m34.7s	−19°35′53″	17	x			PPN	10, 11
18107 − 0710		18h10m47.6s	−07°10′42″	18	x		X	OH/IR	1, 9
18135 − 1456	OH 15.7+0.8	18h13m34.5s	−14°56′19″	−1	x	x	x	PPN	5, 9, 19
18161 − 1713		18h16m07.4s	−17°13′23″	0				?	2
18167 − 1209	OH 18.5+1.4	18h16m47.4s	−12°09′28″	175	x			?	19
18176 − 1848	OH 12.8−1.9	18h17m40.0s	−18°48′33″	13	x	x	x	OH/IR	2, 8, 9
18257 − 1000	OH 21.5+0.5	18h25m43.1s	−10°00′16″	116	x	x	x	OH/IR	2, 5, 9
18276 − 1431	OH 17.7−2.0	18h27m39.8s	−14°31′03″	61	x	x		PPN	15
18281 + 2149	AC Her	18h28m08.8s	+21°49′50″	0				PPN	2
18298 − 2111	AFGL 5501	18h29m51.2s	−21°11′54″	98	x			OH/IR	1
18303 − 0519		18h30m20.5s	−05°19′42″	0				Variable star	2
18310 − 2834		18h31m03.8s	−28°34′46″	−115	x			OH/IR	1
18314 − 2759		18h31m26.2s	−27°59′01″	22	x			?	1
18340 − 0839		18h34m03.5s	−08°39′21″	0	x		X	OH/IR	2, 9
18348 − 0526	OH 26.5+0.6	18h34m52.5s	−05°26′37″	27	x	x	x	OH/IR	2, 5, 7, 9
18437 − 0643	OH 26.4−1.9	18h43m45.3s	−06°43′48″	25	x	x	x	OH/IR	2, 5, 9
18450 − 0148	W 43A	18h45m05.2s	−01°48′18″	34	x	x		PPN	20
18454 + 0250		18h45m29.9s	+02°50′50″	14	x			PMS?	1
18460 − 0254	OH 30.1−0.7	18h46m04.9s	−02°53′55″	99	x	x	x	OH/IR	2, 9
18479 − 2514		18h47m56.4s	−25°14′41″	−30	x			OH/IR	1
18491 − 0207		18h49m10.7s	−02°07′48″	80	x			PPN	17
18526 + 0140		18h52m39.6s	+01°40′51″	−115	x			?	2
18550 + 0130		18h55m02.5s	+01°30′50″	0			X	Variable star	2, 9
18560 + 0638	OH 39.7+1.5	18h56m03.9s	+06°38′50″	20	x	x	x	OH/IR	2, 6
18596 + 0315	OH 37.1−0.8	18h59m36.4s	+03°15′53″	84	x	x	?	PPN	5, 21
19010 + 0526		19h01m05.9s	+05°27′00″	0	x			OH/IR	2
19067 + 0811	OH 42.3−0.1	19h06m43.9s	+08°11′38″	64	x	x	x	PPN	5, 9, 21
19075 + 0921		19h07m34.0s	+09°21′56″	0	x			OH/IR	2, 39
19114 + 0002	AFGL 2343	19h11m25.0s	+00°02′18″	100	x			PPN	1
19127 + 1717		19h12m45.5s	+17°17′25″	16	x			PN	1, 27
19134 + 2131		19h13m26.6s	+21°31′13″	−67		x		PPN	20
19161 + 2343	CRL 2362	19h16m08.6s	+23°43′55″	29	x	x		OH/IR	2
19178 − 2620	CRL 2370	19h17m51.4s	−26°20′16″	5	x		X	OH/IR	2, 9
19190 + 1102		19h19m03.8s	+11°02′56″	−23	x	x		PMS?	1
19192 + 0922	OH 44.8−2.3	19h19m13.1s	+09°22′07″	−72	x	x	x	OH/IR	2, 8, 9

Table 1. continued

IRAS name	Other name	Ra (1950)	Dec (1950)	$V_{\rm lsr}$	OH	H_2O	SiO	Type	Reference
19219 + 0947	VY2−2	19h21m59.3s	+09°48′00″	−60	x			PN	4
19244 + 1115	IRC+10420	19h24m26.8s	+11°15′10″	78	x			Supergiant	34
19283 + 1944	OH 55.0+2.7	19h28m18.1s	+19°44′19″	27	x		X	OH/IR	1, 9
19288 + 2923		19h28m51.4s	+29°23′34″	−40	x	x	x	OH/IR	2, 8
19297 + 2300		19h29m43.5s	+23°00′33″	11	x			PMS?	1
19343 + 2926	M1 92	19h34m17.6s	+29°25′31″	0	x			PPN	35
19352 + 2030	OH 56.4−3.0	19h35m12.7s	+20°30′06″	17	x			OH/IR	1
19511 + 3935		19h51m06.9s	+39°35′34″	23		x		?	1
19566 + 3423		19h56m38.1s	+34°23′20″	−43	x	x		?	1
19576 + 2814	OH 65.7+0.7	19h57m36.3s	+28°14′51″	−59	x			OH/IR	1
20043 + 2653	OH 65.3−2.7	20h04m18.2s	+26°53′30″	−5	x		x	OH/IR	1, 5, 9
20272 + 3535	OH 75.3−1.8	20h27m12.5s	+35°35′35″	−4	x			OH/IR	1
20406 + 2953		20h40m41.5s	+29°53′16″	15	x			?	1, 10, 11
20491 + 4236	OH 83.4−0.9	20h49m09.5s	+42°36′47″	−39	x	x	x	OH/IR	2, 6, 9
21206 + 5145		21h20m38.7s	+51°45′46″	−100	x	x		PMS?	1
21554 + 6204		21h55m29.6s	+62°04′24″	−20	x			?	2
22036 + 5306		22h03m40.0s	+53°06′55″	−40	x			PPN	17
22177 + 5936	OH 104.9+2.4	22h17m43.1s	+59°36′16″	−25	x	x	x	OH/IR	2, 5
22480 + 6002		22h48m00.9s	+60°02′01″	0			X	Supergiant	2, 9
23321 + 6545		23h32m06.3s	+65°45′15″	−15	x			PPN	1, 10, 11
23541 + 7031	M2 56	23h54m06.6s	+70°31′31″	0				PPN	36

References:
1. Likkel (1989), 2. Omont et al. (1993), 3. Silva et al. (1993), 4. Zijlstra et al. (1989), 5. Jewell et al. (1991), 6. Nyman et al. (1986), 7. Nyman et al. (1993), 8. Gomez et al. (1990), 9. This work, 10. Hu et al. (1993a), 11. Hu et al. (1994), 12. Zijlstra et al. (1991), 13. Scarrot et al. (1990), 14. te Lintel Hekkert et al. (1988), 15. Le Bertre et al. (1989), 16. Loup et al. (1990), 17. te Lintel Hekkert (1991), 18. David et al. (1993), 19. van Langevelde et al. (1990), 20. Likkel et al. (1992), 21. Gomez et al. (1994), 22. Slijkhuis et al. (1991), 23. Haikala (1990), 24. van der Veen et al. (1989a), 25. Hrivnak et al. (1988), 26. Hu et al. (1993b), 27. Likkel et al. (1991), 28. Chiar et al. (1993), and Nyman et al. (1993b), 29. te Lintel Hekkert et al. (1992), 30. Forveille et al. (1987), 31. Scarrott & Scarrott (1994), 32. Morris et al. (1982), 33. Waters et al. (1993), 34. Oudmaijer et al. (1994), 35. Bowers & Knapp (1989), 36. Bujarrabal et al. (1992), 37. van de Steene & Pottasch (1993), 38. Bobrowsky et al. (1995), 39. Le Squeren et al. (1992), 40. van der Veen et al. (1989b), 41. Haikala et al. (1994).

Spectra were obtained using a 1024–channel autocorrelator configured to give a velocity coverage of 260 km s^{-1}, and a resolution before smoothing of 0.27 km s^{-1}. Off–line Hanning smoothing was subsequently applied, resulting in a resolution of 0.45 km s^{-1}. Low–order baseline corrections have been applied to the spectra.

3.2. SiO 86 GHz observations

The 86 GHz SiO ($v = 1$, $J = 2-1$) observations were performed on various occasions between 1991 and 1995 using the 15m Swedish–ESO Submillimetre Telescope (SEST) and the Onsala Space Observatory 20 m telescope.

The beamwidth of the SEST is 57″ at 86 GHz, and the pointing accuracy is estimated to be better than 3″ (rms). The telescope was used in a dual beam switch mode with the source alternately placed in the two beams, a method that yields very flat baselines. The beam separation was about 11′.5. The aperture efficiency of the telescope at 86 GHz is 62%, which gives a conversion factor of 25 Jy K^{-1}.

The receiver was a dual (linear) polarization Schottky receiver with a typical system temperature above the atmosphere of 400 − 500 K (SSB). Only the horizontally polarized receiver was used. Calibration was done with a standard chopper wheel method and the flux values are estimated to be accurate to ±20%.

Spectra were taken with an acousto optical spectrometer (AOS) with a bandwidth of 86 MHz (resulting in a velocity coverage of 300 km s^{-1}), a channel separation of 43 kHz, and a resolution of 80 kHz. The spectra were subsequently smoothed by adding the spectrometer channels together four by four, resulting in a velocity resolution of about 0.6 km s^{-1}.

The Onsala 20 m telescope has a beamwidth of 43″ at 86 GHz, and the pointing accuracy is estimated to be better than 3″ (rms). The telescope was used in a dual beam switch mode with a beam separation of about 11′.5. The aperture efficiency of the telescope at 86 GHz is 0.5, which gives a conversion factor of 18 Jy K^{-1}.

The receiver was a horizontally, linearly polarized SIS receiver with a typical system temperature above the atmosphere of 400−500 K (SSB). Calibration was done with a standard chopper wheel method and the flux values are estimated to be accurate to ±20%.

Spectra were taken with a multichannel filterbank with a bandwidth of 64 MHz, resulting in a velocity coverage of 220 km s^{-1}, and a channel separation of 250 kHz, which corresponds to a velocity resolution of 0.87 km s^{-1}.

4. Results

The results of the SiO maser observations are presented in Table 2, and spectra of the detected sources are shown in Fig. 1. The observations were made mainly in the SiO ($v = 1$, $J = 2-1$ and $v = 2$, $J = 1-0$) lines. Only a few selected sources were observed in the SiO ($v = 1$, $J = 1-0$) line. In total 28 sources were detected in SiO emission of which 13 are new detections. The detection rate for the $v = 2$, $J = 1-0$ line is 23% compared with 15% for the $v = 1$, $J = 2-1$ line, in agreement with the conclusion of Nyman et al. (1993a) that the $v = 1$, $J = 2-1$ line is relatively weak in objects with cool envelopes. A few objects, however, were detected in the $J = 2-1$ line but not in the $J = 1-0$ line, possibly due to the time variability of the SiO maser emission. Most of the detected objects are OH/IR stars. Only two objects classified as PPNe were detected (OH $231.8+4.2$ and OH $42.3-0.1$), and one, OH $15.7+0.8$, was tentatively detected. No SiO masers were found towards any of the PNe because most likely the SiO molecules will be photodissociated near their central stars.

We will only discuss the detections and non–detections in a qualitative way, i.e., we will for instance not compare the relative intensities of the various transitions, since the data were taken at different epochs, in only one linear polarization, and for the SiO ($v = 2$, $J = 1-0$) transition a few sources were observed during unstable weather. Most of the PPNe and PNe were observed during good weather conditions, however, and we do not believe that we failed to make a detection because of the weather.

Apart from the tentative detection towards OH $15.7+0.8$, which is classified as a PPNe, SiO masers were found to be associated only with variable objects. Two of these are classified as PPNe (OH $231.8+4.2$ and OH $42.3-0.1$). The rest are OH/IR stars with the exception of two objects with uncertain classification (IRAS $08357-1013$ and IRAS $16029-3041$). The latter are however most likely OH/IR objects based on their double–peaked OH line profiles, the 10 μm dust features, the single–peaked energy distributions, and the late–type (M) central stars. Their classification is uncertain because of the low value of the IRAS variability indices and the lack of monitoring observations reported in the literature. However, observations in the infrared and of the OH masers reported by various authors show variability both in the infrared and of the OH emission (e.g. Allen et al. 1977; Fouqué et al. 1992; te Lintel Hekkert et al. 1991; Le Squeren et al. 1979; Slootmaker et al. 1985).

5. SiO masers in proto–planetary nebulae

5.1. OH 231.8+4.2

OH 231.8 is a bipolar nebula (e.g. Reipurth 1987) with a high–velocity outflow seen in OH and CO, and it has a rich molecular spectrum (Morris et al. 1982, 1987). SiO maser emission has been detected by Barvainis & Clemens (1984), Morris et al. (1987), Jewell et al. (1991), and in this work. The central star is a long–period variable of spectral class M with a period of about 680 days (Feast et al. 1983; Cohen et al. 1985). Cohen et al. demonstrated the presence of a blue companion, and the bipolar outflow is therefore most likely caused by mass transfer between the central stars. The SiO maser is probably associated with the long–period variable.

5.2. OH 42.3–0.1

OH 42.3 belongs to a class of objects where the velocity width of the H_2O maser emission is larger than that of the OH emission and it has been suggested that they are in the early stages of becoming high–velocity outflow sources (Gomez et al. 1994). SiO maser emission was detected by Jewell et al. (1991), and in this work. The OH maser emission is variable with a period of more than 2000 days.

Other objects where the velocity width of the H_2O maser emission is larger than that of the OH emission are OH $37.1-0.8$ and OH $12.8-0.9$ (Gomez et al. 1994). OH 37.1 is a star with non–variable OH emission (Herman & Habing 1985). It was tentatively detected in SiO by Jewell et al. (1991), but not by Gomez et al. (1990), Nyman et al. (1993a), or in this work, and we therefore regard it as a non–detection. No SiO maser has been found toward OH 12.8 (Jewell et al. 1991).

5.3. OH 19.2–1.0

OH 19.2 was not included in our sample, but it has been detected in SiO emission by Jewell et al. (1991). It has a peculiar OH maser spectrum with at least four peaks, and maps of the OH emission has been interpreted in terms of a bipolar outflow (Chapman 1988). The OH emission is variable with a period of about 600 days (Chapman 1988).

5.4. OH 15.7+0.8

OH 15.7 is a non–variable OH/IR star (Herman & Habing 1985) with a double peaked energy distribution. It was tentatively detected by Jewell et al. (1991) and in this work, and regarded as detected by Nyman et al. (1993a) but with a low signal to noise ratio. The possible maser components cover a similar velocity range in the different observations. No SiO masers have been found towards other objects of this type, e.g. OH $17.7-2.0$ and OH $18.5+1.4$ (this work; Jewell et al. 1991).

Table 2. SiO maser observations. The epoch is given in JD+2440000, rms and peak intensity in Jy, and integrated intensities in units of 10^{-20} W m^{-2}. Only the peak flux is given for tentatively detected sources. An asterisk(*) in front of the rms value of the SiO ($v = 2$, $J = 1 - 0$) observations indicate that the calibration is uncertain due to unstable weather. An asterisk (*) in front of the epoch of the SiO (2-1) observations indicate that they were made with the Onsala 20 m telescope

Source	SiO $v = 1$, $J = 1 - 0$				SiO $v = 2$, $J = 1 - 0$				SiO $v = 1$, $J = 2 - 1$			
	Epoch	rms	peak	Int.	Epoch	rms	peak	Int.	Epoch	rms	peak	Int.
$01304 + 6211$									*9344	0.4		
$03206 + 6521$									*9343	0.4		
$03293 + 6010$									*9344	0.4	2.6	2.9
$04361 + 2547$									8528	0.9		
$06319 - 0501$					9251	1.4			9387	0.3		
$06530 - 0213$					9251	1.3			8528	0.6		
$07027 - 7934$					9251	1.6			9275	0.5		
$07131 - 0147$					9251	1.1			8528	0.4		
$07180 - 1314$					9252	1.9			9387	0.5	3.0	5.1
$07399 - 1435$	9253	2.1	5.1		9249	1.4	8.2	4.4	8528	0.5	5.0	6.4
$07536 - 2830$	9253	2.1	10.4	8.4	9251	1.3	9.6	3.4	9274	1.2	7.5	18.6
$07559 - 5859$					9251	1.8			9387	0.6		
$08005 - 2356$	9253	2.1			9249	0.9			8528	0.6		
$08357 - 1013$	9253	2.4	13.0	9.2	9251	1.6	11.6	8.3	9274	0.9	3.8	4.2
$09371 + 1212$	9253	2.2			9249	1.4			8723	0.8		
$09429 - 2148$	9253	5.1	70.2	38.0	9251	2.6	55.0	21.1	9274	1.0	27.0	26.8
$10197 - 5750$	9253	1.8			9248	0.6			8723	0.5		
$10197 - 5750$									9274	1.0		
$11385 - 5517$	9253	1.2			9249	1.1			8723	0.5		
$11516 - 6201$					9251	1.7			9274	0.9		
$12358 - 6323$									9282	1.4		
$14086 - 0730$	9253	2.3	18.7	9.7	9252	1.6	7.0	3.1	9387	0.8	10.0	13.0
$14122 - 5947$									9387	0.5		
$14341 - 6211$									9282	1.1		
$15405 - 4945$	9253	2.0			9247	*0.9			8527	0.6		
$16029 - 3041$	9253	2.5	15.6	8.5	9249	2.2	41.0	11.9	8531	0.7	10.0	6.3
$16086 - 5255$									9282	1.1		
$16235 - 4832$	9253	2.3			9251	2.1			8530	0.6		
$16342 - 3814$	9253	2.0			9248	0.8			8527	0.5		
$16559 - 2957$					9250	1.5			8527	0.8		
$16594 - 4656$					9251	1.8			8911	0.5		
$17103 - 6302$	9253	2.3			9247	*1.0			8530	0.6		
$17106 - 3046$					9249	0.9			9275	1.2		
$17118 - 2952$					9251	2.4			8723	0.7		
$17150 - 3224$					9249	1.4			8911	0.8		
$17150 - 3754$					9249	1.0			8530	0.6		
$17163 - 3907$					9251	1.4			8530	0.6		
$17195 - 2710$									9282	1.0		
$17207 - 2856$					9249	0.9			8530	0.6		
$17221 - 3038$					9249	1.2			8531	0.6		
$17233 - 2602$									9282	1.0		
$17292 - 2727$					9251	2.2			8786	0.7		
$17317 - 2743$					9251	2.3			8786	0.8		
$17347 - 3139$					9251	1.4			8531	0.6		
$17360 - 3012$	9253	5.2	54.6	21.0	9250	2.7	39.8	19.2	8786	0.8	6.3	8.6
$17371 - 2747$	9253	1.7			9248	1.2			8527	0.5		
$17371(OH)$					9252	1.2						
$17375 - 2759$					9248	0.7			8531	0.5		
$17375(OH)$					9252	1.3						
$17375 - 3000$					9249	1.2			8533	0.6		

Table 2. continued

Source	SiO $v = 1$, $J = 1 - 0$				SiO $v = 2$, $J = 1 - 0$				SiO $v = 1$, $J = 2 - 1$			
	Epoch	rms	peak	Int.	Epoch	rms	peak	Int.	Epoch	rms	peak	Int.
17385 − 3332									9282	1.1		
17393 − 2727					9249	1.4						
17404 − 2713									9282	1.0		
17411 − 3154	9253	4.1	108.1	33.6	9250	3.1	152.9	115.5	8786	0.7	20.0	27.3
17423 − 1755					9249	1.2			8530	0.5		
17433 − 1750					9251	2.0			8531	0.5		
17433 − 1750									9382	1.0		
17443 − 2519					9250	1.3			8786	0.8		
17443 − 2949					9249	1.3			8531	0.6		
17459 − 3057					9250	2.1			8786	0.8	3.8	8.6
17484 − 1511					9251	1.9			8723	0.8		
17505 − 3143	9253	2.6	6.6	1.4	9251	1.2	3.9	2.3	8563	1.0		
17516 − 2526					9251	2.0			8723	0.8		
17534 + 2603									8723	0.9		
17565 − 2035					9252	1.7			8563	1.0		
17579 − 3121					9249	1.0			9275	1.2		
17580 − 3511					9248	1.5			8531	0.6		
18016 − 2743									9382	1.0		
18025 − 3906					9249	1.4			9282	1.0		
18044 − 1947					9252	2.1			8533	0.8		
18055 − 1833					9250	1.7			8533	0.7		
18071 − 1727					9250	2.3			8533	0.8		
18081 − 0338					9251	1.8			8563	1.1		
18095 + 2704									*9338	0.4		
18105 − 1935									9282	1.0		
18107 − 0710	9253	3.0	5.5		9252	1.5	9.0	2.1	8563	1.2		
18135 − 1456	9253	1.5	5.1		9247	0.7			8563	1.0		
18135 − 1456									*9343	0.6		
18161 − 1713					9252	1.7			8564	1.1		
18167 − 1209					9249	1.5			8911	0.4		
18176 − 1848	9253	2.2	17.2	9.8	9252	1.6	16.8	8.7	8564	1.1		
18257 − 1000	9253	2.6			9251	1.6	27.7	14.2	8564	1.0		
18276 − 1431	9253	1.6			9247	*1.0			8531	0.8		
18276 − 1431									*9344	0.4		
18281 + 2149									*9336	0.4		
18298 − 2111					9251	1.8			8533	0.7		
18303 − 0519					9252	2.1			8786	0.7		
18310 − 2834					9252	1.2			8563	1.1		
18314 − 2759					9251	1.4			8563	1.1		
18340 − 0839					9251	1.9			8786	0.6	2.5	4.0
18348 − 0526	9253	2.3	44.5	11.8	9247	*5.8	67.5	21.1	8786	0.8		
18437 − 0643	9253	2.0	5.5		9252	1.8	9.3	3.6	8533	0.9		
18450 − 0148					9248	1.3			9275	1.0		
18454 + 0250					9252	2.1			8563	1.1		
18460 − 0254	9253	3.0			9251	1.7	26.9	12.2	9275	1.2		
18479 − 2514					9251	1.2			8533	0.8		
18491 − 0207					9249	1.6			8531	0.5		
18526 + 0140									9990	0.4		
18550 + 0130					9251	1.4			9275	1.2	5.3	20.1
18560 + 0638	9253	2.7	40.2	25.4	9252	3.1	73.3	56.7	9275	1.3		
18596 + 0315	9253	1.9			9252	1.4			*9344	0.5		
19010 + 0527					9251	1.9			9275	1.2		
19010 + 0527									*9342	0.5		
19067 + 0811	9253	3.6	18.6	11.0	9251	1.5	20.7	13.5	9276	1.2		
19067 + 0811									*9342	0.8		

Table 2. continued

Source	SiO $v = 1$, $J = 1 - 0$				SiO $v = 2$, $J = 1 - 0$				SiO $v = 1$, $J = 2 - 1$			
	Epoch	rms	peak	Int.	Epoch	rms	peak	Int.	Epoch	rms	peak	Int.
19075 + 0921					9251	2.0			9275	1.3		
19075 + 0921									*9342	0.5		
19114 + 0002					9251	2.0			8563	1.1		
19127 + 1717					9251	1.3			8563	1.2		
19127 + 1717									*9344	0.4		
19134 + 2131									*9339	0.4		
19161 + 2343									*9340	0.8		
19178 − 2620	9253	2.4	19.5	13.4	9251	1.4	26.1	21.0	8533	0.8	16.3	17.5
19190 + 1102					9252	2.2			9275	1.2		
19192 + 0922	9253	2.8	17.6	4.7	9252	1.7	19.9	5.2	9276	1.1	7.5	6.5
19219 + 0947					9248	1.4			8530	0.6		
19244 + 1115					9248	1.8			8531	0.6		
19283 + 1944	9253	3.1	10.1	2.1	9251	2.4	13.3	4.8	9276	1.2		
19283 + 1944									*9342	0.8		
19288 + 2923									*9339	0.6		
19297 + 2300									*9342	0.6		
19343 + 2926									*9336	0.3		
19352 + 2030									9990	0.6		
19511 + 3935									*9338	1.2		
19566 + 3423									*9340	0.6		
19576 + 2814									*9344	0.3		
20043 + 2653									*9343	0.3	1.2	1.5
20272 + 3535									*9339	0.6		
20406 + 2953									*9340	0.5		
20491 + 4236									*9337	0.4	3.3	5.9
21206 + 5145									*9339	0.5		
21554 + 6204									*9339	0.4		
22036 + 5306									*9335	0.4		
22177 + 5936									*9340	0.5		
22480 + 6002									*9340	0.8	5.8	27.3
23321 + 6545									*9342	0.7		
23541 + 7031									*9344	0.5		

5.5. SiO maser properties of the detected PPNe

The SiO masers in OH 231.8, OH 42.3, OH 19.2, and the tentatively detected OH 15.7 all have properties similar to those of SiO masers seen towards Mira variables and OH/IR stars: line widths of $5 - 10$ km s^{-1} and center velocities close to the mean velocity of the OH emission.

OH 19.2 is observed to be bipolar and the OH and H_2O maser properties of OH 42.3 can be modeled in terms of a bipolar outflow (Gomez et al. 1994). Their SiO maser emission can therefore be explained in the same way as for OH 231.8 (Sect. 5.1): the central objects are binary systems where one of the components is a variable red giant presently undergoing mass loss. The bipolar nebula is shaped by the mass transfer between the two stars and the SiO maser is associated with the variable star. Schwarz et al. (1995) made a survey of SiO masers in dusty symbiotic systems, and emission was found only in systems with wide orbits. Their observations show that SiO masers may exist near variable stars also in binary systems.

OH 15.7 has probably very recently left the AGB. Its H_2O maser emission has been very irregular over the past years and recently disappeared (Engels 1997), indicating that the mass loss rate is irregular and decreasing.

5.6. Detection rates and comparison to OH/IR stars

Only two SiO masers were clearly detected in the objects classified as PPNe in our sample, and one, OH 15.7+0.8, was tentatively detected. This is considerably fewer than towards the OH/IR stars. The low detection rate of SiO emission towards PPNe could be explained if these sources are situated at larger distances than OH/IR objects. However, distance estimates for the various types of objects indicate that they, on the average, are located at similar distances. It is also possible to estimate whether the non-detections are significant by comparing the SiO maser fluxes with the total energy fluxes, since it is likely

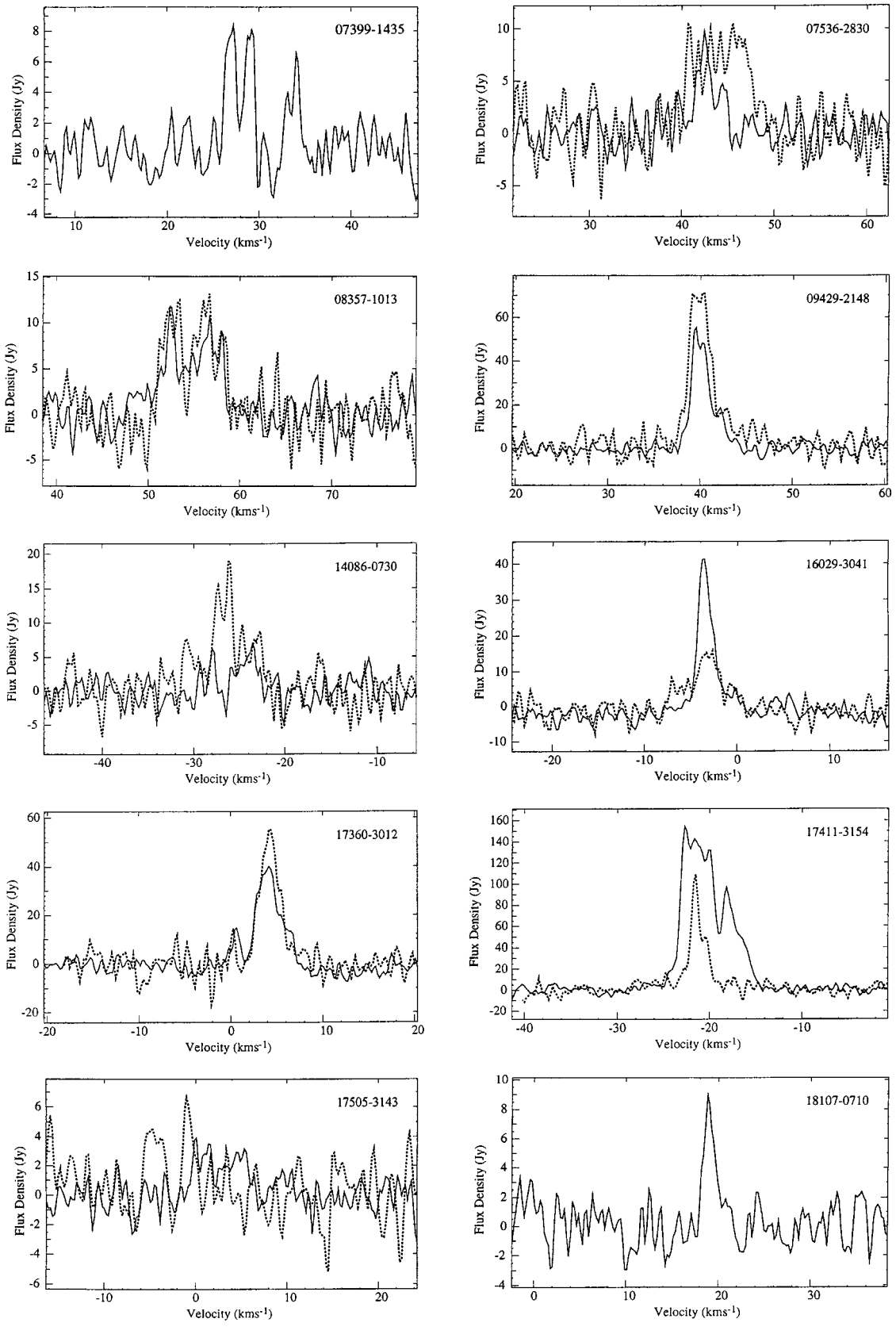

Fig. 1. a) The SiO 43 GHz ($v = 1$, $J = 1 - 0$) and ($v = 2$, $J = 1 - 0$) spectra of the detected sources. The $v = 2$ spectra are shown with solid lines, the $v = 1$ spectra with dotted lines. **b)** The SiO 86 GHz ($v = 1$, $J = 2 - 1$) spectra of the detected sources. The velocity scale is given with respect to the local standard of rest

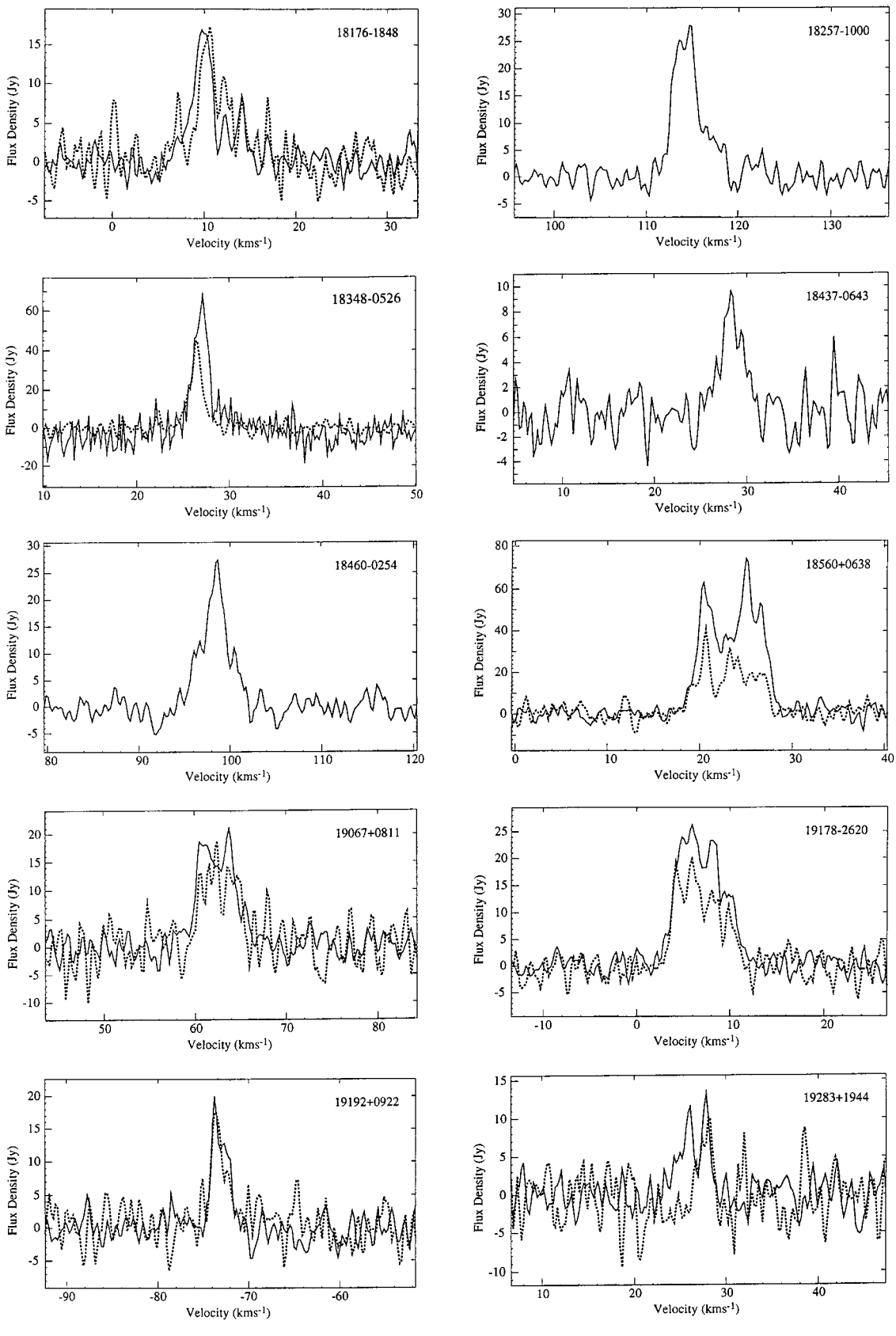

Fig. 1. a) continued

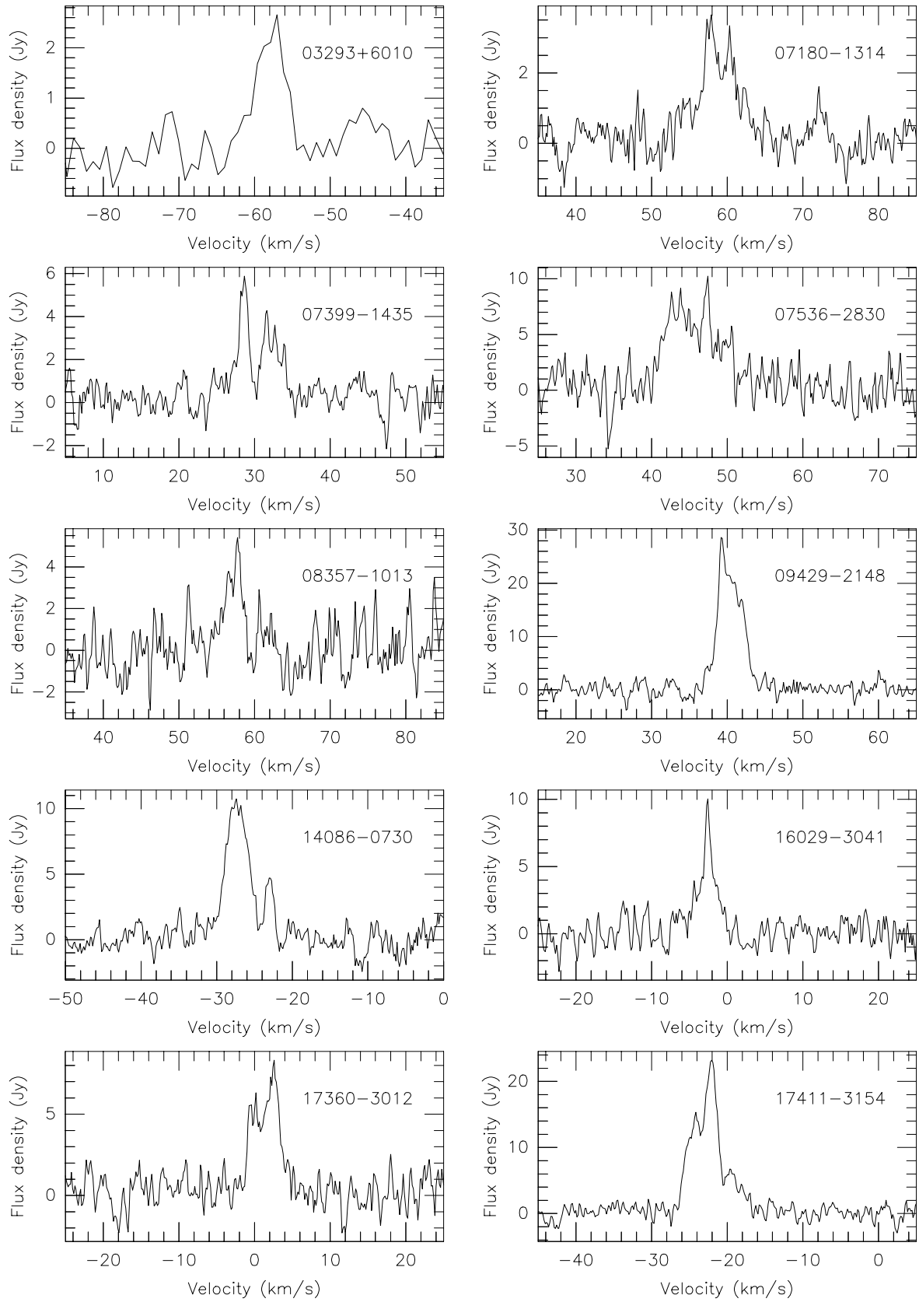

Fig. 1. b) continued

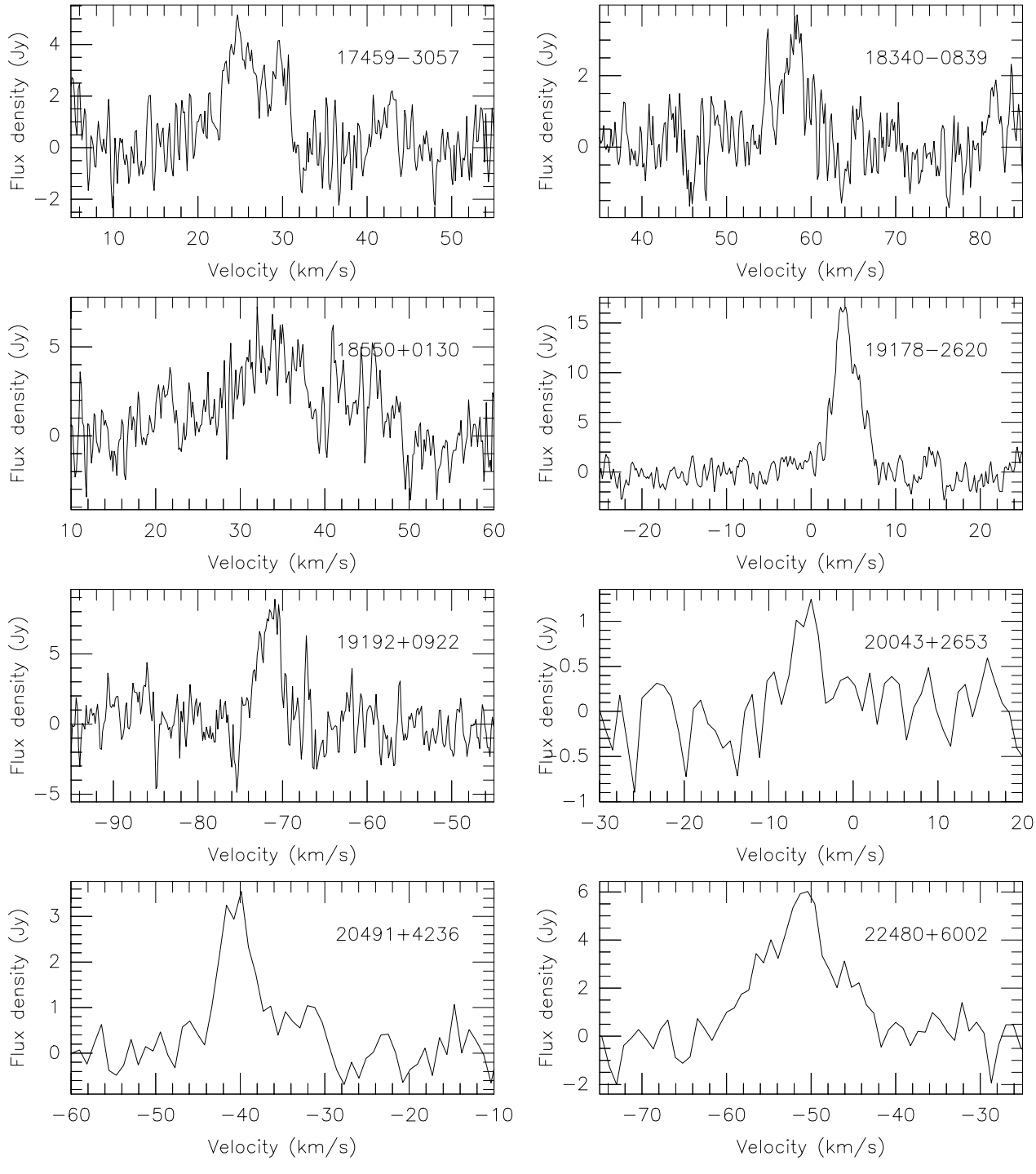

Fig. 1. b) continued

that the luminosities of OH/IR stars are similar to those of PPNe. In Fig. 2 we have plotted the SiO ($v = 2$, $J = 1-0$) energy flux versus the far infrared energy flux (calculated from the IRAS intensities). For the OH/IR stars the far infrared energy flux should be a good approximation to the total energy flux, since they mainly radiate in the far infrared, but for the PPNe and PNe it is only a lower limit. Many PPNe have far infrared energy fluxes comparable to those of the detected OH/IR stars, indicating that the absence of SiO emission is real and not caused by a distance effect.

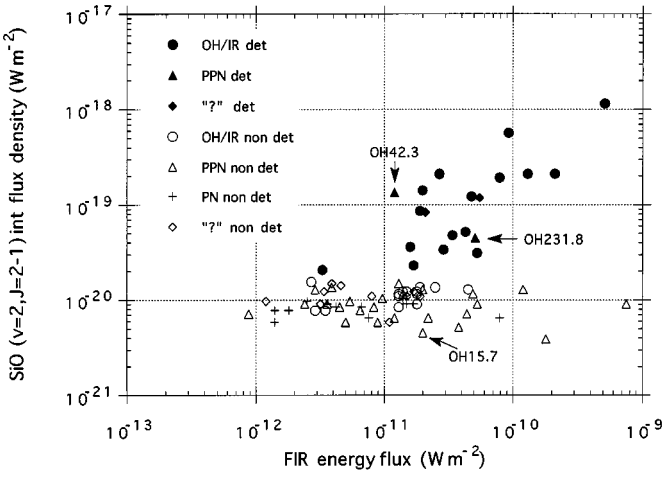

Fig. 2. SiO ($v = 2$, $J = 1 - 0$) integrated flux densities plotted as function of the far infrared energy flux. Detections, as well as upper limits, are included. The upper limits to the SiO integrated flux densities were calculated in the same way as in Nyman et al. (1993a). The objects are divided into OH/IR stars, PPNe, PNe, and unclassified sources ("?") according to Table 1. Note that the FIR energy flux is only an upper limit to the total energy flux of the PPNe and PNe. OH 15.7 was not detected in the $v = 2$ transition and only tentatively detected in the $v = 1$ transition. (Nyman et al. 1993a, reported an integrated flux density of 2 10^{-20} W m^{-2} in the $v = 1$ transition)

6. SiO masers in an IRAS two–color diagram

An IRAS two–color diagram can be used to roughly identify stars in different stages of their evolution (cf. Olnon et al. 1984; Bedijn 1987; van der Veen & Habing 1988). Due to the different properties of their dust shells, OH/IR stars, PPNe, and PNe occupy slightly different regions in the diagram (although there is also an overlap), and the diagram has been found to be especially useful in the selection of PPNe (e.g., Hu et al. 1993a). Figure 3 shows a plot of $[F_{60}/F_{25}]$ versus $[F_{25}/F_{12}]$ for the sources in this sample and also from previous observations by Gomez et al. (1990), Nyman et al. (1993a), and the OH/IR objects detected by Jewell et al. (1991). The colors are defined from the IRAS fluxes in the following way: $[F_{\lambda1}/F_{\lambda2}] = 2.5 \times \log(F_{\lambda1}/F_{\lambda2})$.

As was also found by Gomez et al. (1990) very few sources are detected beyond $[F_{25}/F_{12}] = 1.2$. Only two sources with redder colors have been found to have SiO masers: OH 231.8+4.2 and OH 15.7+0.8 which are discussed in the previous section. Bedijn (1987) suggests that sources with $[F_{25}/F_{12}] > 1.2$ have ceased their mass loss and are surrounded by a detached envelope.

To study in more detail how the detection rate of SiO masers changes with IRAS colors, we have taken the data from our observations as well as from the papers listed above and calculated the detection rates as function of $[F_{25}/F_{12}]$. The data were separated into bins of 0.4 units in IRAS color, except for the last bin which is three times larger to contain more objects. The results are shown in Table 3. The statistical error in the detection rate is given within parenthesis in Table 3, and was calculated assuming that the detected sources have a Poisson distribution. As found by Gomez et al. (1990) there is a gradual decrease in detection rate with increasing IRAS color. The gradual decrease is partly due to a small decrease in the detection rate of the OH/IR stars, but mainly due to an increase in the number of PPNe and unclassified sources with increasing $[F_{25}/F_{12}]$.

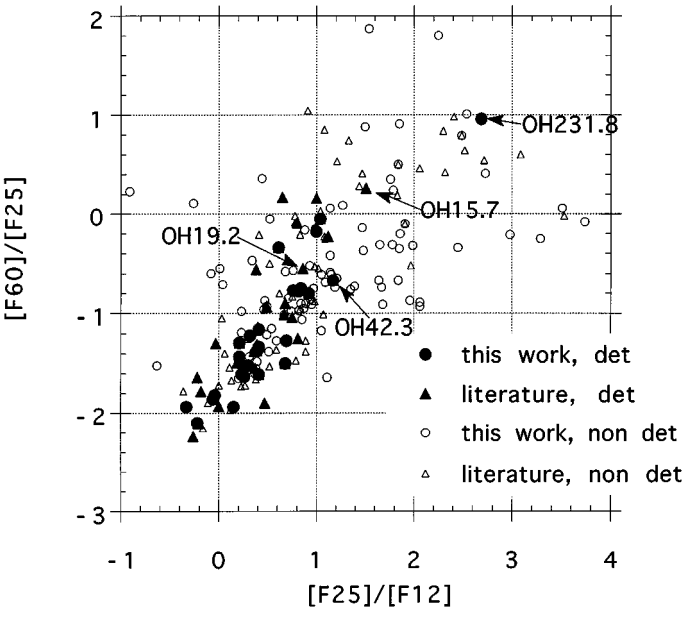

Fig. 3. IRAS two–color diagram of detected and non–detected sources in our sample and from previous observations by Gomez et al. (1990), Nyman et al. (1993a), and Jewell et al. (1991)

7. The relation between SiO masers and the properties of the central stars

Unlike OH and H_2O masers, SiO masers are believed to be located not in the expanding circumstellar envelope, but in a region called the extended atmosphere, i.e., between the photosphere of the star and the dust formation point. This is a complex region with both outflowing and infalling gas as seen in infrared lines of OH and H_2O (Hinkle et al. 1982), and there is also evidence of periodic shocks, driven by stellar pulsations, passing through (Willson 1982). There are several arguments supporting the view that SiO masers are located here:

Table 3. Detection rates

	Our sample and data from literature, all objects			Our sample, all objects			Our sample, OH/IR objects only		
$[F_{25}/F_{12}]$	No. of obj.	No. of det.	Det rate (%)	No. of obj.	No. of det.	Det rate (%)	No. of obj.	No. of det.	Det rate (%)
$-0.4 - 0.0$	22	15	68 (18)	6	4	67 (33)	3	3	100 (56)
$0.0 - 0.4$	46	21	45 (10)	21	12	55 (16)	18	11	61 (18)
$0.4 - 0.8$	43	18	42 (10)	21	9	43 (14)	10	8	80 (28)
$0.8 - 1.2$	46	11	24 (17)	27	6	22 (9)	12	5	42 (19)
$1.2 - 1.6$	13	1	8 (8)	9	0	0	0		
$1.6 - 2.0$	19	0	0	16	0	0	0		
$2.0 - 2.4$	7	0	0	3	0	0	0		
$2.4 - 2.8$	8	1	12 (12)	5	1	20 (20)	0		
$2.8 - 4.0$	6	0	0	4	0	0	0		

1. SiO masers have been detected in vibrational states up to 6800 K above the ground state, and the masers must thus be close to the star (Cernicharo et al. 1993).
2. In the expanding wind most of the silicon is incorporated into dust grains, leaving little SiO to produce maser emission.
3. There is no correlation between envelope expansion velocities and the width of the SiO maser lines, and there is no correlation between mass loss rates and SiO photon fluxes (Nyman & Olofsson 1986).
4. Interferometric observations of SiO masers show that they are located near the central star, and also inside the dust formation zone (Diamond et al. 1994; Danchi et al. 1995).

Observational evidence that SiO masers appear when the star first starts to pulsate is given by Haikala et al. (1994). In their Fig. 6a the number of all detected SiO masers as function of IRAS LRS class is shown. A large number of SiO masers are found in classes 14–17 with a peak at class 15, but no masers were found in classes 18 and 19. Van der Veen & Habing (1988) showed that objects in LRS classes 17–19 are normally non–variable stars with photospheric temperatures larger than 2000 K, whereas classes 14–16 consist of variable stars with a small amount of circumstellar material. This indicates that there is a close correlation between variability and the probability of finding SiO masers.

During the subsequent evolution along the AGB, SiO masers have a very high detection rate, and they are found in Mira variables and OH/IR stars with the characteristics given above. Hall et al. (1990) found a strong correlation between the presence of SiO masers and the optical variability of the central star. In their sample, stars with a visual amplitude larger than 2.5 mag were almost invariably detected in SiO.

In this work we show that also at the end of the AGB there is a close correlation between variability and the presence of SiO masers. SiO masers were found only towards variable objects, including the detected PPNe, but with the possible exception of OH 15.7 (tentatively detected, Sect. 5) which however is an object that only very recently may have evolved into a PPNe and shows irregular mass loss.

It is not evident how variability and SiO masers are connected. Most likely it is the variability that produces the extended atmosphere through mass motions. Here the conditions are favorable for the formation of SiO masers. When the variability decreases, or even stops, the conditions in the masing region change, prohibiting strong SiO masers. Since the latter most probably is a very sensitive process, it is not clear how dramatic the changes in the physical conditions are required to be to give this effect. It may be, once our understanding of the SiO maser mechanism has improved, that the SiO masers can be used as sensitive probes of the changing atmospheric conditions during the very last phase of AGB evolution. Apart from the disappearance of mass motions, also the increase in effective temperature of the central star during the post–AGB evolution will eventually increase the photodissociation rate of the SiO molecules, making the existence of masers impossible.

Acknowledgements. This research has made use of the Simbad database, operated at CDS, Strasbourg, France. We thank the referee, J. Alcolea, for helpful comments that improved the paper. The Swedish–ESO Submillimetre Telescope, SEST, is operated jointly by ESO and the Swedish National Facility for Radioastronomy, Onsala Space Observatory at Chalmers University of Technology. Parkes Observatory is part of the Australia Telescope which is funded by the Commonwealth of Australia for operation as a National Facility managed by CSIRO.

References

Allen D.A., Hyland A.R., Longmore A.J., Caswell J.L., Goss W.M., Haynes R.F., 1977, ApJ 217, 108
Barvainis R., Clemens D.P., 1984, AJ 89, 1833
Bedijn P.J., 1987, A&A 186, 136

Bobrowsky M., Zijlstra A.A., Grebel E.K., Tinney C.G., te Lintel Hekkert P., van de Steene G.C., Likkel L., Bedding T.R., 1995, ApJ 446, L89
Bowers P.F., Knapp G.R., 1989, ApJ 347, 325
Bujarrabal V., Alcolea J., Planesas P., 1992, A&A 257, 701
Cernicharo J., Bujarrabal V., Santaren J.L., 1993, ApJ 407, L33
Chapman J.M., 1988, MNRAS 230, 415
Chiar J.E., Whittet D.C.B., Aitken D.K., Roche P.F., Smith C.H., Walker H.J., Whitelock P.A., Wright C., 1993, ApJ 409, 404
Cohen M., Dopita M.A., Schwartz R.D., Tielens A.G.G.M., 1985, ApJ 297, 702
Danchi W.C., Bester M., 1995, Ap&SS 224, 339
David P., Le Squeren A.M., Sivagnanam P., 1993, A&A 277, 453
Diamond P.J., Kemball A.J., Junor W., Zensus A., Benson J., Dhawan V., 1994, ApJ 430, L61
Engels D., 1997, in Planetary Nebulae, Habing H. & Lamers H. (eds.) IAU 180. Kluwer (in press)
Feast M.W., Catchpole R.M., Whitelock P.A., Roberts G., Spencer Jones J., Carter B.S., 1983, MNRAS 203, 1207
Forveille T., Morris M., Omont A., Likkel L., 1987, A&A 176, L13
Fouqué P., Le Bertre T., Epchtein N., Guglielmo F., Kerschbaum F., 1992, A&AS 93, 151
Gomez Y., Moran J.M., Rodriguez L.F., 1990, Rev. Mex. Astron. Astrofis. 20, 55
Gomez Y., Rodriguez L.F., Contreras M.E., Moran J.M., 1994, Rev. Mex. Astron. Astrofis. 28, 97
Haikala L.K., 1990, A&AS 85, 875
Haikala L.K., Nyman L.–Å., Forsström V., 1994, A&AS 103, 107
Hall P.J., Allen D.A., Troup E.R., Wark R.M., Wright A.E., 1990, MNRAS 243, 480
Herman J., Habing H.J., 1985, A&AS 59, 523
Hinkle K.H., Hall D.N.B., Ridgway S.T., 1982, ApJ 252, 697
Hrivnak B.J., Kwok S., Volk K.M., 1988, ApJ 331, 832
Hu J.Y., Slijkhuis S., de Jong T., Jiang B.W., 1993a, A&AS 100, 413
Hu J.Y., Slijkhuis S., Nguyen–Q–Rieu, de Jong T., 1993b, A&A 273, 185
Hu J.Y., te Lintel Hekkert P., Slijkhuis S., Baas F., Sahai R., Wood P., 1994, A&AS 103, 301
Jewell P.R., Snyder L.E., Walmsley C.M., Wilson T.L., Gensheimer P.D., 1991, A&A 242, 211
Le Bertre T., Epchtein N., Gouiffes C., Heydari–Malayeri M., Perrier C., 1989, A&A 225, 417
Le Sqeuren A.M., Baudry A., Brillet J., Darchy B., 1979, A&A 72, 39
Le Squeren A.M., Sivagnanam P., Dennefeld M., David P., 1992, A&A 254, 133
Lewis B.M., 1989, ApJ 338, 234
Likkel L., 1989, ApJ 344, 350
Likkel L., Forveille T., Omont A., Morris M., 1991, A&A 246, 153
Likkel L., Morris M., Maddalena R.J., 1992, A&A 256, 581
Loup C., Forveille T., Nyman, L.–Å., Omont A., 1990, A&A 227, L29
Morris M., Bowers P.F., Turner B.E., 1982, ApJ 259, 625
Morris M., Guilloteau S., Lucas R., Omont A., 1987, ApJ 321, 888
Nyman L.–Å., Hall, P.J., Le Bertre T., 1993a, A&A 280, 551
Nyman L.–Å., Johansson L.E.B., Booth R.S., 1986, A&A 160, 352
Nyman L.–Å., Olofsson H., 1986, A&A 158, 67
Nyman, L.–Å., Olofsson H., Rogers C., Heske A., Sahai R., 1993b, in Mass Loss on the AGB and Beyond, Schwarz H. (ed.), ESO Conference and Workshop proceedings No. 46, p. 451
Olnon F.M., Baud B., Habing H.J., de Jong T., Harris S., Pottasch S.R., 1984, ApJ 278, L41
Oudmaijer R.D., Geballe T.R., Waters L.B.F.M., Sahu K.C., 1994, A&A 281, L33
Omont A., Loup C., Forveille T., te Lintel Hekkert P., Habing H., Sivagnanam P., 1993, A&A 267, 515
Reipurth B., 1987, Nat 325, 787
Scarrott S.M., Rolph C.D., Wolstencroft R.D., Walker H.J., Sekiguchi K., 1990, MNRAS 245, 484
Scarrott S.M., Scarrott R.M.J., 1994, MNRAS 268, 615
Schwarz H.E., Nyman L.–Å., Seaquist E.R., Ivison R.J., 1995, A&A 303, 833
Silva A.M., Azcarate I.N., Pöppel W.G.L., Likkel L., 1993, A&A 275, 510
Slijkhuis S., Hu J.Y., de Jong T., 1991, A&A 248, 547
Slootmaker A., Herman J., Habing H.J., 1985, A&AS 59, 465
te Lintel Hekkert P., 1991, A&A 248, 209
te Lintel Hekkert P., Caswell J.L., Habing H.J., Haynes R.F., Norris R.P., 1991, A&AS 90, 327
te Lintel Hekkert P., Chapman J.M., Zijlstra A.A, 1992, ApJ 390, L23
te Lintel Hekkert P., Habing H.J., Caswell J.L., Norris R.P., Haynes R.F., 1988, A&A 202, L19
van de Steene G.C.M., Pottasch S.R., 1993, A&A 274, 895
van der Veen W.E.C.J., Geballe T.R., Habing H.J., van Langevelde H.J., 1989a, A&A 216, L1
van der Veen W.E.C.J., Habing H.J., 1988, A&A 194, 125
van der Veen W.E.C.J., Habing H.J., Geballe T.R., 1989b, A&A 226, 108
van Langevelde H.J., van der Heiden R., van Schooneveld C., 1990, A&A 239, 193
Volk K., Cohen M., 1989, AJ 98, 931
Waters L.B.F.M., Waelkens C., Mayor M., Trams N.R., 1993, A&A 269, 242
Willson, L.A., 1982, in Pulsations in Classical and Cataclysmic Variable Stars, Cox J.P., Hansen J. (eds.). Boulder, JILA, p. 284
Winfrey S., Barnbaum C., Morris M., Omont A., 1994, BAAS 26, 1382
Zijlstra A.A., Gaylard M.J., te Lintel Hekkert P., Menzies J., Nyman L.–Å., Schwarz H.E., 1991, A&A 243, L9
Zijlstra A.A., te Lintel Hekkert P., Pottasch S.R., Caswell J.L., Ratag M., Habing H.J., 1989, A&A 217, 157